

Acceleration disturbances and requirements for ASTROD I

Sachie Shiomi¹ and Wei-Tou Ni^{1,2,3}

¹Department of Physics, National Tsing Hua University, Hsinchu, Taiwan 30013 ROC

²Purple Mountain Observatory, Chinese Academy of Sciences, Nanjing 210008 China

³National Astronomical Observatories, Chinese Academy of Sciences, Beijing 100012 China

Abstract.

ASTRODynamical Space Test of Relativity using Optical Devices I (ASTROD I) mainly aims at testing relativistic gravity and measuring the solar-system parameters with high precision, by carrying out laser ranging between a spacecraft in a solar orbit and ground stations. In order to achieve these goals, the magnitude of the total acceleration disturbance of the proof mass has to be less than $10^{-13} \text{ m s}^{-2} \text{ Hz}^{-1/2}$ at 0.1 mHz. In this paper, we give a preliminary overview of the sources and magnitude of acceleration disturbances that could arise in the ASTROD I proof mass. Based on the estimates of the acceleration disturbances and by assuming a simple control-loop model, we infer requirements for ASTROD I. Our estimates show that most of the requirements for ASTROD I can be relaxed in comparison with Laser Interferometer Space Antenna (LISA).

PACS numbers: 04.80.Nn, 04.80.-y, 95.55.Ym

1. Introduction

ASTRODynamical Space Test of Relativity using Optical Devices (ASTROD) [1, 2] aims at testing relativistic gravity, measuring the solar-system parameters with high precision and detecting gravitational waves from massive black holes and galactic binary stars. The concept of ASTROD is to put two spacecraft in separate solar orbits and carry out laser interferometric ranging with Earth reference stations (e.g. a spacecraft at the Earth-Sun L1/L2 points). A simple version of ASTROD, ASTROD I[‡], has been studied as the first step to ASTROD [3, 4]. ASTROD I employs one spacecraft in a solar orbit and carries out interferometric ranging and pulse ranging with ground stations. The main scientific goals of ASTROD I are to test relativistic gravity and the fundamental laws of spacetime with three-order-of-magnitude improvement in sensitivity and to improve the solar, planetary and asteroid parameter determination by 1 to 3 orders of magnitude. The technological goal of ASTROD I is to prepare for the ASTROD mission.

[‡] ASTROD I was previously referred to as Mini-ASTROD (for instance in [3]).

The acceleration disturbance goal of the ASTROD I proof mass is $10^{-13} \text{ m s}^{-2} \text{ Hz}^{-1/2}$ at frequency ν of 0.1 mHz. The power spectral density of the allowed level of the acceleration noise is shown in figure 1. Assuming a 10 ps one-way timing accuracy (3 mm ranging accuracy) and the acceleration noise of $10^{-13} \text{ m s}^{-2} \text{ Hz}^{-1/2}$ at frequency of about 0.1 mHz, a simulation for 400 days (350–750 days after launch) showed that ASTROD I could determine the relativistic parameters γ and β , and the solar quadrupole parameter J_2 to levels of 10^{-7} , 10^{-7} and 10^{-8} , respectively [5]. In the simulation, (i) the timing noise is modeled as Gaussian random noise; (ii) unknown acceleration noise is modeled to have Gaussian random magnitude with zero mean and with standard deviation $10^{-15} \text{ m s}^{-2}$ and to have its direction changed randomly every 4 h (equivalent to $10^{-13} \text{ m s}^{-2} \text{ Hz}^{-1/2}$ for $\nu \sim 0.1 \text{ mHz}$ assumed as the requirement of the drag-free system) and (iii) five range points are taken each day (at 0.2 d interval). Longer term systematic effects will be studied in a future paper. This simulation agrees with the scientific goals of ASTROD I. The timing uncertainty of event timer reaches 3 ps in satellite laser ranging at present. Space qualified versions of similar accuracy are under development. For a ranging uncertainty of 3 mm in a distance of $3 \times 10^{11} \text{ m}$ (2 AU), the laser/clock frequency needs to be known to one part in 10^{14} . This can be set as a requirement of the space laser/clock or a requirement for laser frequency monitoring through ground clock and modeling. As to ground station jitter, monitoring to an accuracy of 3 mm is required and can be achieved. The atmospheric effects on laser propagation will be monitored and subtracted to mm-level by using 2-color (2-wavelength) ranging (one color for pulse ranging and one for interferometric ranging). These measurement uncertainties are not cumulative in the range determination while the acceleration disturbances accumulate in time in the geodesic deviations. In order to achieve the acceleration disturbance goal, a drag-free control system using capacitive sensors will be employed.

In order to decide on detailed designs of the accelerometer for ASTROD I, we have to know the sources and magnitude of acceleration disturbances that could arise in the accelerometer. In this paper, we carry out analyses, mainly based on existing literature on acceleration disturbances for other gravitational missions (LISA [7, 8] and the LISA Pathfinder [6, 9]), to give a preliminary overview of the acceleration disturbance to the ASTROD I proof mass. Based on the analyses, we infer some of the requirements for the designs of the ASTROD I payload and spacecraft. Also, we compare parameter values we have assumed in the analyses with those for LISA to confirm the feasibility of the requirements for ASTROD I.

First, we will give an overview of the ASTROD I configuration (section 2) and the control-loop model we assumed (section 3). Then, we will estimate the magnitude of acceleration disturbances and requirements for ASTROD I in sections 4 to 8, and compare the requirements of ASTROD I with LISA in section 9.

2. ASTROD I spacecraft configuration

The ASTROD I spacecraft has a cylindrical shape with diameter 2.5 m and height 2 m. Its cylindrical side is covered by solar panels. The cylindrical axis is perpendicular to the orbit plane and the telescope is set to point toward a ground laser station. The effective area of receiving sunlight is about 5 m^2 and it can generate power that is larger than 500 W. The total mass of the spacecraft is about 350 kg and that of payload is 100–120 kg (see [4, 10] for more detailed descriptions of the configuration). The orbit distance from the Sun varies from about 0.5 AU to 1 AU (figure 2 of [10]).

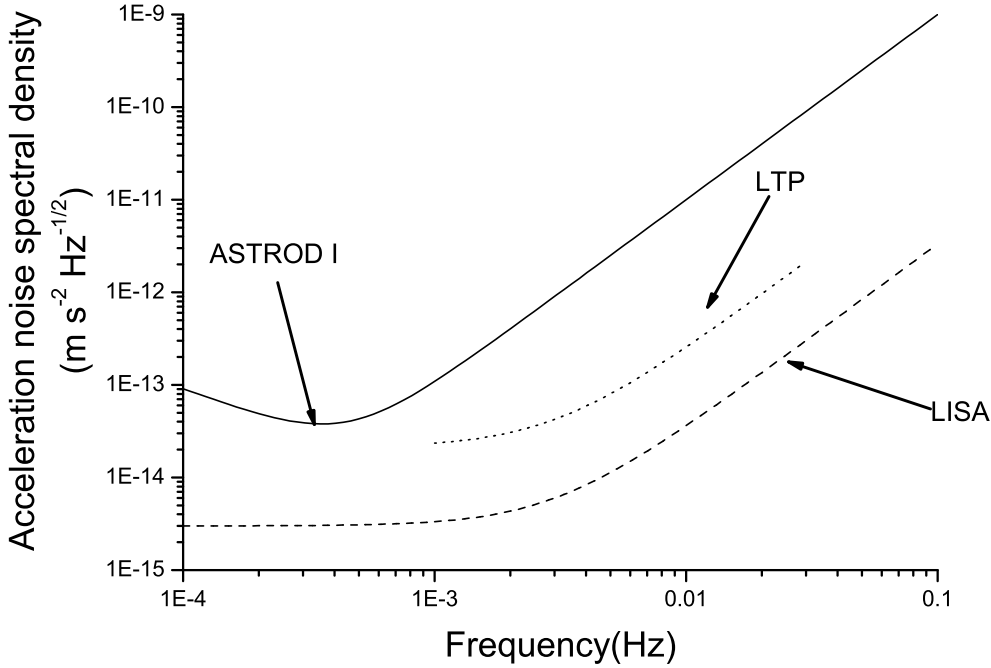


Figure 1. Acceleration noise spectral density requirements for ASTROD I. The LISA Technology Package (LTP) requirements [6] and LISA requirements [7] are illustrated in the figure for comparison.

The proof mass ($m_p = 1.75$ kg) is a rectangular parallelepiped ($50 \times 50 \times 35$ mm³)[§] made from Au-Pt alloy (density $\rho = 2 \times 10^4$ kg m⁻³). The six sides of the proof mass are surrounded by electrodes mounted on the housing for capacitive sensing and control. The gap between each side of the proof mass and the opposing electrode is 2 mm. Assumed values for the capacitance and voltages are listed in table 1.

3. Control-loop model

Various acceleration disturbances would act on the proof mass in different ways. In order to infer how these different kinds of acceleration disturbances would contribute to the total acceleration disturbance of the proof mass, we tentatively assume a simple single-mass and single-axis control-loop model [11, 12]. The diagram is shown in figure 2. The relative difference between the displacement disturbance amplitudes of the proof mass and of the spacecraft, $X_{ps} = X_p - X_s$, with position readout noise X_{nr} , is measured by the position displacement sensor. The output of this sensor is converted to acceleration disturbance f_r , by a transfer function $R (\equiv \omega_R^2)$. This acceleration is supplied to the thruster and the output acceleration disturbance with thruster noise N_t is applied to the spacecraft. The spacecraft also experiences acceleration disturbances by coupling to the proof mass with a coupling constant K and external environmental

[§] This is the current design of the proof mass. A cylindrical shape is also considered as an alternative design of the proof mass.

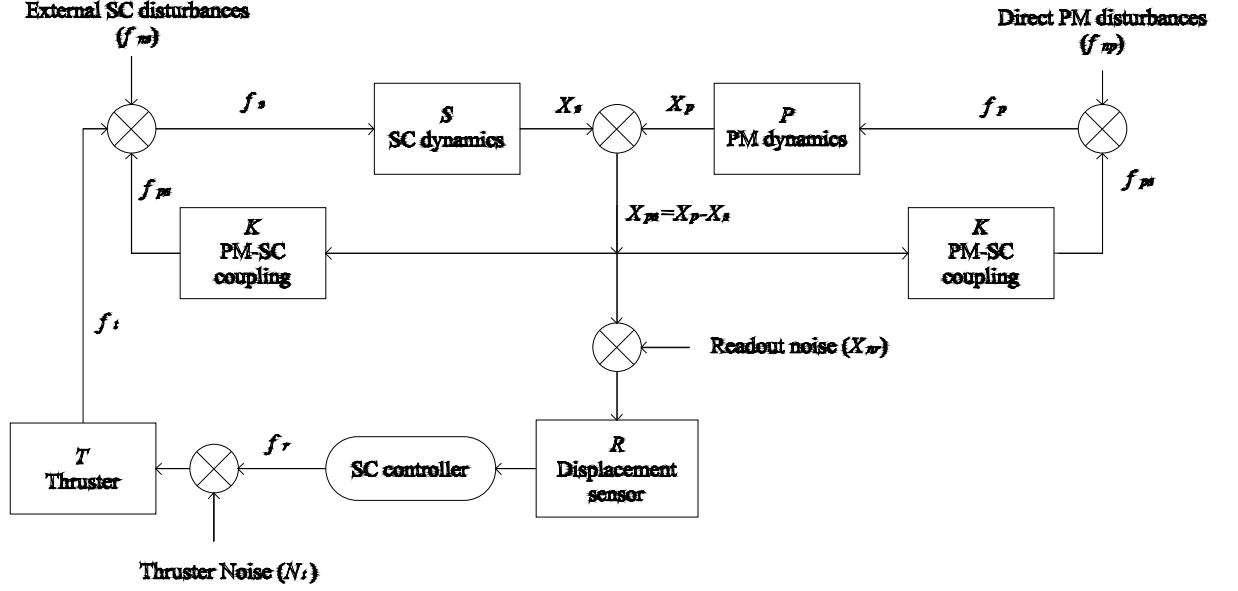


Figure 2. Control loop model. SC and PM denote spacecraft and proof mass, respectively.

disturbances (f_{ns}) that work directly on the spacecraft. The total acceleration of the spacecraft f_s is converted to the position noise X_s with a transfer function S .

We consider only the sensitive axis of the proof mass without actuation. The proof mass would experience disturbances by spacecraft-proof mass coupling and environmental disturbances f_{np} (see section 5). The total acceleration disturbance of the proof mass f_p is converted to the displacement disturbance X_p with a transfer function P .

From this control-loop model, we obtain the following linear loop equations [13, 14]:

$$f_r = R(X_{ps} + X_{nr}) \quad (1)$$

$$f_t = T(f_r + N_t) \quad (2)$$

$$f_s = f_{ns} + f_t - (m_p/M_{sc})f_{ps} \quad (3)$$

$$f_p = f_{np} + f_{ps} \quad (4)$$

$$f_{ps} = KX_{ps} \quad (5)$$

$$X_s = Sf_s \quad (6)$$

$$X_p = Pf_p \quad (7)$$

By solving these equations for X_p , and assuming $S = P = \omega^{-2}$ and $u \equiv STR$ ($= T\omega_R^2\omega^{-2}$; T is nominally 1 and its effects are absorbed in R and N_t), we obtain (e.g. [11, 12, 13, 14]):

$$f_p \approx X_{nr}(-K) + f_{np} + (f_{ns} + TN_t)K\omega^{-2}u^{-1} \quad (8)$$

where $\omega = 2\pi\nu$. This acceleration disturbance has to be less than the acceleration noise goal of $10^{-13} \text{ m s}^{-2} \text{ Hz}^{-1/2}$ at $\nu = 0.1 \text{ mHz}$.

We will estimate the values of the direct acceleration disturbances of the spacecraft (f_{ns} and the thruster noise TN_t) in section 4 and of the proof mass (f_{np}) in sections 5 and 6, and the stiffness K in section 7. We will discuss the requirements for X_{nr} and u in section 8.

4. Direct acceleration disturbances of the spacecraft

The spacecraft would be affected by environmental disturbances that stem from, for example, solar radiation pressure, solar wind and micrometeorite impacts. Among these sources of disturbances, solar radiation pressure is considered to be the major contributor to the acceleration disturbances (section 7 of [8]). The contribution from solar wind might be comparable to radiation pressure, but the spectral behavior of the solar wind is not well known.

By assuming a perfectly reflecting surface of the spacecraft, acceleration noise caused by fluctuation in solar irradiance δW_0 is $f_{ns, srp} = \frac{4}{3}(A_{sc}\delta W_0/M_{sc}c)$, where A_{sc} is the area of the spacecraft facing the Sun, M_{sc} is the mass of the spacecraft and c is the speed of light in vacuum. From the data of the VIRGO experiment on SOHO [15], fractional fluctuation in solar irradiance is $\delta W_0/W_0 \approx 2.8 \times 10^{-3} \text{ Hz}^{-1/2}$ at 0.1 mHz (figure 6 of [15]). Assuming that $\delta W_0/W_0$ is the same at 0.5 AU , and taking a total irradiance of 5500 W m^{-2} , the area of 5 m^2 and a mass of 350 kg , we obtain $f_{ns, srp} = 9.8 \times 10^{-10} \text{ m s}^{-2} \text{ Hz}^{-1/2}$.

The impact rate of 1-ng meteorites on the ASTROD I spacecraft (its surface area is 25.5 m^2) is about 7 events per day or about 0.08 mHz ||. The average velocity of meteorites is 18 km s^{-1} in an Earth frame near the Earth (figure 7.2-30 of [8]). An impact of 1-ng meteorite with the average velocity of 18 km s^{-1} on the surface of the spacecraft (350 kg) without reflection produces a linear velocity increment of about $5 \times 10^{-11} \text{ m s}^{-1}$. Smaller meteorites have larger flux (figure 7.2-29 of [8]), but their impacts on velocity changes are smaller. Therefore, the contribution to the acceleration disturbances at 0.1 mHz seems insignificant, in comparison with the effect of solar radiation pressure. However, because such discrete changes could directly affect the ASTROD I experiment, the impact effects have to be studied carefully in detail.

In addition to the acceleration noise from the environmental disturbances, the spacecraft would suffer from the thruster noise. A force fluctuation of $10 \mu\text{N Hz}^{-1/2}$ in thruster corresponds to the acceleration disturbance of $TN_t = 2.8 \times 10^{-8} \text{ m s}^{-2} \text{ Hz}^{-1/2}$.

Therefore, the rss (root-sum-square) of these acceleration disturbances is:

$$f_{ns} + TN_t \approx 2.8 \times 10^{-8} \text{ m s}^{-2} \text{ Hz}^{-1/2} \quad (9)$$

at 0.1 mHz , dominated by the thruster noise. As per [7], LISA requires a force fluctuation to be less than a few $\mu\text{N Hz}^{-1/2}$. However, recent studies for the LISA Pathfinder indicate that force noise up to $0.1 \text{ mN Hz}^{-1/2}$ at 0.1 mHz can be tolerated by increasing the gain [16]; the LISA study team is designing high gain loops and the requirement has been relaxed¶.

|| This rate was tentatively estimated from the meteorite flux/mass distribution used by the LISA study team (figure 7.2-29 of [8]).

¶ This is a comment from one of the referees.

5. Direct acceleration disturbances of the proof mass

Direct proof-mass acceleration disturbances can be classified into two categories depending on their origins [13, 14]: environmental disturbances (f_{nep}) and proof-mass sensor back-action acceleration disturbances (f_{nbp}). The former includes disturbances related to magnetic effects (f_{m1} , f_{m2} , f_{m3} , f_{L1} and f_{L2}), impact effects (by cosmic ray (f_c) and residual gas (f_{rg})), temperature dependent effects (radiometric and outgassing effects (f_{re} and f_{og}) and thermal radiation pressure (f_{tr})) and gravity gradients caused by thermal distortion of the spacecraft (f_{gg}). The latter is originated from voltage fluctuations (f_{b1} and f_{b2}), charge fluctuations (f_{b3} and f_{b4}), readout electronics (f_{ba}), patch field voltages (f_{pe}) and thermal voltage noise by dielectric losses (f_{dl}).

Parameter values and physical constants used for the estimations are listed in tables 1 and 2, respectively. Table 3 provides a summary of the expressions used to estimate the direct proof-mass acceleration disturbances and the estimated values. The disturbances noted as f_{m1} , f_{m2} , f_{L1} , f_{L2} , f_c , f_{rg} , f_{re} , f_{tr} , f_{gg} and f_{b1} - f_{b4} in table 3 correspond to A_1 - A_6 and A_8 - A_{14} in [14], respectively⁺. We will briefly explain each disturbance below.

5.1. Magnetostatic interaction

The lowest order force on a proof mass with a magnetic moment \vec{M}_p in an external magnetic field \vec{B} is given by $\vec{F}_m = \vec{\nabla}(\vec{M}_p \cdot \vec{B})$ [17]. The magnetic moment of the proof mass is a vector sum of the remanent moment \vec{M}_r and the induced moment [18]: $\vec{M}_p = \vec{M}_r + (\chi_m V_p / \mu_0) \vec{B}$, where χ_m and V_p are magnetic susceptibility and the volume of the proof mass, respectively; $\mu_0 = 1.26 \times 10^{-6} \text{ N A}^{-2}$ is the permeability of vacuum. The external magnetic field would be given by the superposition of the interplanetary magnetic field \vec{B}_{ip} and a local magnetic field \vec{B}_{sc} . Dominant terms in acceleration of the proof mass due to the induced magnetic moment produce acceleration disturbances noted f_{m1} and f_{m2} in table 3, where ξ_m is a scaling factor for possible suppression by magnetic shielding.

The average interplanetary magnetic field at 1 AU from the Sun varies from 10^{-9} to $3.7 \times 10^{-8} \text{ T}$ [19]. Ulysses data obtained near 1 AU from the Sun (figure 9 of [20]) showed a $\nu^{-2/3}$ dependence of the variation in the interplanetary magnetic field and δB_{ip} can be inferred to be about $10^{-7} \text{ T Hz}^{-1/2}$ at 0.1 mHz. As the behavior of δB_{ip} at 0.5 AU from the Sun is uncertain, we use a somewhat higher value of $\delta B_{ip} = 4 \times 10^{-7} \text{ T Hz}^{-1/2}$ (see footnote in section 5.2). According to the formulation studies for LISA and the implementation work of the LISA Pathfinder, batteries and micro-thrusters are the principal suspects of the origins of the local magnetic field in LISA*. We need elaborate modeling works to estimate the magnitude of local magnetic field. Here, we use the same values used in analyses for LISA [14, 21]: $B_{sc} \approx 8 \times 10^{-7} \text{ T}$, $\delta B_{sc} = 10^{-7} \text{ T Hz}^{-1/2}$ and $|\vec{\nabla} B_{sc}| \approx 3 B_{sc} r_m^{-1} \approx 3 \times 10^{-6} \text{ T m}^{-1}$ (where $r_m = 0.75 \text{ m}$). Silvestri et al. have reported that the magnetic susceptibility of five samples ranged from -2.8×10^{-5} to -2.1×10^{-5} for two of them without traceable iron contamination and from $+1.1 \times 10^{-5}$ to $+8.8 \times 10^{-5}$ for the rest samples with a trace of iron [22].

⁺ The acceleration disturbance due to laser photon radiation pressure, noted as A_7 in [14], would not arise in ASTROD I, as the laser beam is not to be injected directly on the surface of the ASTROD I proof mass.

* This is a comment from one of the referees.

Table 1. Parameter values used in the acceleration noise estimates

$\nu = 0.1$ mHz	ASTROD I
Proof Mass (PM)	
Mass: m_p [kg]	1.75
Density: ρ [kg m ⁻³]	2×10^4
Cross section: A_p [m ²]	0.050×0.035
Temperature: T_p [K]	293
Fluctuation of temperature difference	
across PM and housing: δT_d [K Hz ^{-1/2}]	1.0×10^{-5}
Maximum charge build-up: q [C]	10^{-12}
Fluctuation in charge: δq [C Hz ^{-1/2}]	6.1×10^{-15}
Magnetic susceptibility: χ_m	5×10^{-5}
Magnetic remanent moment: $ \vec{M}_r $ [A m ²]	1×10^{-7}
Residual gas pressure: P [Pa]	10^{-5}
Electrostatic shielding factors: ξ_e	10
Magnetic shielding factors: ξ_m	1
Spacecraft (SC)	
Mass: M_{sc} [kg]	350
Velocity: v [m s ⁻¹]	4×10^4
Thruster noise [μ N Hz ^{-1/2}]	10
Area facing the Sun: A_{sc} [m ²]	5
Fluctuation of temperature in SC: δT_{sc} [K Hz ^{-1/2}]	0.2
Capacitive sensing	
Capacitance: C_x [pF]	6
Capacitance to ground: C_g [pF]	6
Total capacitance: C [pF]	$(6C_g \approx) 36$
Gap: d [mm]	2
Asymmetry in gap across opposite sides of PM: Δd [μ m]	10
Average voltage across opposite faces: V_{x_0} ($\equiv (V_{x_1} + V_{x_2})/2$) [V]	0.1
Proof mass bias voltage: V_{M0} [V]	0.6
Voltage difference between V_{x_0} and voltage to ground: V_{0g} [V]	0.05
Voltage difference between opposing faces: V_d [V]	0.01
Fluctuation of voltage difference across opposite faces:	
δV_d [V Hz ^{-1/2}]	10^{-4}
Residual dc bias voltage on electrodes: V_0 [V]	0.1
Loss angle: δ	10^{-5}
Magnetic fields	
Local magnetic field: B_{sc} [T]	8×10^{-7}
Local magnetic field gradient: $ \vec{\nabla} B_{sc} $ [T m ⁻¹]	3×10^{-6}
Fluctuation in local magnetic field: $ \delta B_{sc} $ [T Hz ^{-1/2}]	1×10^{-7}
Interplanetary magnetic field: B_{ip} [T]	1.2×10^{-7}
Interplanetary magnetic field gradient: $ \delta B_{ip} $ [T Hz ^{-1/2}]	4×10^{-7}
Gradient of time-varying magnetic field: $ \vec{\nabla}(\delta B) $ [T m ⁻¹ Hz ^{-1/2}]	4×10^{-8}
Cosmic rays	
Impact rate: λ [s ⁻¹]	30
Mass of positron: m [kg]	1.7×10^{-27}
Incident energy: E_d [J]	$(200 \text{ MeV} \Rightarrow) 3.2 \times 10^{-11}$
Gravity gradients	
Source mass: M_{dis} [kg]	1 in f_{gg} and 0.03 in a_{gg}
Distance from the source mass: x [m]	0.5 in f_{gg} and 0.05 in a_{gg}
Thermal expansion coefficient: $CTE(\text{Aluminium})$ [K ⁻¹]	2.5×10^{-5}
Patch field	
Multiplicative factor: γ	5
Patch field voltage: V_{pe} [V]	0.1

Table 2. Physical constants used in the estimation

	Symbols	Values used in the estimations
Elementary charge	e	1.6×10^{-19} C
Permeability of vacuum	μ_0	1.26×10^{-6} N A ⁻²
Permittivity of vacuum	ε_0	8.9×10^{-12} F m ⁻¹
Speed of light in vacuum	c	3.0×10^8 m s ⁻¹
Boltzmann constant	k_B	1.38×10^{-23} J K ⁻¹
Stefan-Boltzmann constant	σ	5.7×10^{-8} W m ⁻² K ⁻⁴
Gravitational constant	G	6.7×10^{-11} m ³ kg ⁻¹ s ⁻²

Table 3. The estimated values for the proof-mass acceleration disturbances at the frequency of 0.1 mHz. PM and rss denote proof mass and root-sum-square, respectively. The values are in units of 10^{-15} m s⁻² Hz^{-1/2}. See sections 5 and 6, and tables 1 and 2 for notation.

[10^{-15} m s ⁻² Hz ^{-1/2}]		Expressions	ASTROD I
(a) PM environmental acceleration disturbances			
f_{m1}	Magnetic	$\frac{2\chi_m}{\rho\mu_0\xi_m} \vec{\nabla} B_{sc} \delta B_{sc}$	1.2
f_{m2}	Magnetic	$\frac{\sqrt{2}\chi_m}{\rho\mu_0\xi_m} \vec{\nabla} B_{sc} \delta B_{ip}$	3.4
f_{m3}	Magnetic	$\frac{1}{\sqrt{2}m_p} \vec{M}_r \vec{\nabla}(\delta B) $	1.6
f_{L1}	Magnetic	$\frac{v}{\xi_c m_p} \delta q B_{ip}$	0.0017
f_{L2}	Magnetic	$\frac{v}{\xi_c m_p} q \delta B_{ip}$	0.91
f_c	Cosmic rays	$\sqrt{\frac{4m E_d \lambda}{m_p^2}}$	0.0015
f_{rg}	Residual gas	$2 \sqrt{\frac{P A_p}{m_p^2} (3k_B T_p m_N)^{1/4}}$	0.74
f_{re}	Radiometric	$\frac{A_p P}{2m_p} \frac{\delta T_d}{T_p}$	0.17
f_{og}	Outgassing	$10 f_{re}$	1.7
f_{tr}	Thermal radiation	$\frac{8}{3} \frac{\sigma A_p}{m_p c} T_p^3 \delta T_d$	0.13
f_{gg}	Gravity gradients	$\frac{2GM_{dis}}{x^2} CTE \cdot \delta T_{sc}$	2.7
rss($f_{m1} - f_{gg}$) $\equiv f_{nep}$			5.2
(b) PM sensor back-action acceleration disturbances			
f_{b1}	$\delta V_d \times V_{0g}$	$\frac{C_x}{m_p d} \frac{C_q}{C} V_{0g} \delta V_d$	1.4
f_{b2}	$\delta V_d \times q$	$\frac{1}{m_p d} \frac{C_x}{C} q \delta V_d$	4.8
f_{b3}	$\delta q \times V_d$	$\frac{1}{m_p d} \frac{C_x}{C} V_d \delta q$	2.9
f_{b4}	$\delta q \times q$	$\frac{1}{m_p d} \frac{C_x}{C^2} \frac{\Delta d}{d} q \delta q$	0.040
f_{ba}	Readout electronics	(see table 1 of [37])	1.8
f_{pe}	Patch fields	$\frac{1}{m_p d} \frac{C_x}{C} V_{pe} \delta q$	29
f_{dl}	Dielectric losses	$\sqrt{2} \frac{C_x}{m_p d} V_0 \delta v_{diel}$	1.6
rss($f_{b1} - f_{dl}$) $\equiv f_{nbp}$			30
rss($f_{m1} - f_{dl}$) $\equiv f_{np}$			30

Lower susceptibility may be achievable by controlling the manufacturing process of the alloy. The requirement for LISA is $\chi_m = 3 \times 10^{-6}$ [23]. We use a somewhat moderate value of $\chi_m = 5 \times 10^{-5}$. Assuming $\xi_m = 1$ as per [13, 14], we obtain $f_{m1} = 1.2 \times 10^{-15} \text{ m s}^{-2} \text{ Hz}^{-1/2}$ and $f_{m2} = 3.4 \times 10^{-15} \text{ m s}^{-2} \text{ Hz}^{-1/2}$ at 0.1 mHz.

Acceleration disturbance due to the magnetic remanent moment is given by f_{m3} listed in table 3 (equation 4(c) of [18]), where $\Delta(\delta B)$ is time-varying magnetic field gradients. According to measurements by Gill et al., magnetic remanent moment of three 4.2-cm 70/30 Au-Pt alloy cubes (one of them was 73/27 Au-Pt alloy) ranged from $3.5 \times 10^{-9} \text{ A m}^2 \text{ kg}^{-1}$ to $3.1 \times 10^{-8} \text{ A m}^2 \text{ kg}^{-1}$ [24]. By scaling the largest measured remanent moment by weight, it is $5.4 \times 10^{-8} \text{ A m}^2$ for a 1.75-kg proof mass. By using a somewhat relaxed value of $1 \times 10^{-7} \text{ A m}^2$ and $|\nabla(\delta B)| = 4 \times 10^{-8} \text{ T m}^{-1} \text{ Hz}^{-1/2}$ [18], which is a factor of four higher than the assumed requirement for LISA in [23], we obtain $f_{m3} = 1.6 \times 10^{-15} \text{ m s}^{-2} \text{ Hz}^{-1/2}$ at 0.1 mHz. In the error estimates for LISA [23], magnetic remanent moment of $2 \times 10^{-8} \text{ A m}^2$ is used.

5.2. Lorentz force

The proof mass in orbit would be charged up by cosmic-ray impacts [25, 7]. As the charged proof mass moves through the interplanetary magnetic field (\vec{B}_{ip}) with a velocity v of about $4 \times 10^4 \text{ m s}^{-1}$, it experiences the Lorentz force: $\vec{F}_L = q\vec{v} \times \vec{B}_{ip}$, where q is the built-up charge. Acceleration disturbances due to the fluctuation of the charge build-up (δq) in the proof mass and of the average interplanetary magnetic field are given by f_{L1} and f_{L2} (see table 3), respectively, where ξ_e is an electrostatic shielding factor; in the rest frame of the proof mass, the motion of the proof mass through the interplanetary magnetic field generates an electrostatic field.

By assuming the Poisson distribution of cosmic-ray impacts, the average charge fluctuation spectral density can be defined as $\delta q(\omega) \equiv \sqrt{2e\dot{q}}/\omega$. For the frequency ($\nu = (2\pi)^{-1}\omega$) of 0.1 mHz and the effective charging rate (\dot{q}) of 288 e s^{-1} , which was estimated for a LISA proof-mass (46-mm cube) by a simulation using GEANT 4 toolkit [26], we obtain $\delta q(\omega) = 6.1 \times 10^{-15} \text{ C Hz}^{-1/2}$. Using this value, $\xi_e = 10$ and $B_{ip} = 1.2 \times 10^{-7} \text{ T}$, we obtain $f_{L1} = 1.7 \times 10^{-18} \text{ m s}^{-2} \text{ Hz}^{-1/2}$ at 0.1 mHz. The maximum value of B_{ip} at 1 AU is about $3 \times 10^{-8} \text{ T}$. We tentatively use four times the maximum value as B_{ip} at 0.5 AU, by assuming $1/(\text{distance})^2$ dependence of B_{ip} ‡. Because the volume of the ASTROD I proof-mass is about 10 % smaller than the LISA proof mass, the charging rate for ASTROD I might be smaller than the value for LISA. Bao et al. are working on simulations to estimate the charging rates for ASTROD I [27]. Stebbins et al. use $\xi_e = 100$, which is one order of magnitude larger than the value we used here, in the current error estimates for LISA [23]. Taking a nominal maximum build-up charge $q = 10^{-12} \text{ C}$, which is one order of magnitude larger than the value used in the error estimates for LISA [13, 14, 23], we obtain $f_{L2} = 9.1 \times 10^{-16} \text{ m s}^{-2} \text{ Hz}^{-1/2}$.

5.3. Cosmic-ray impacts

Some cosmic rays get stopped in the proof mass and deposit momentum [25, 7]. Assuming the Poisson distribution of cosmic ray impact, spectral density of momentum transfer (p) is $2p^2\lambda$, where λ is the fluctuation in the impact rate [25]. The acceleration

‡ The solar dipole field at 0.5 AU is less than $\sim 10^{-10} \text{ T}$. The main magnetic field at 0.5 AU to 1 AU is due to the influence of solar winds which attenuate with $(\text{distance})^2$.

disturbance due to the fluctuation in the impact rate is given by f_c , listed in table 3. The impact rate was inferred from simulations done for LISA; by adding the effects of all stopped particles (protons and helium) and taking into account their directions, the acceleration disturbance by momentum transfer was estimated to be $\approx 2 \times 10^{-18} \text{ m s}^{-2} \text{ Hz}^{-1/2}$ for a LISA proof mass [25]. This corresponds to a disturbance due to momentum transfer by protons (mass $m = 1.7 \times 10^{-27} \text{ kg}$), with an impact rate of $\sim 30 \text{ s}^{-1}$, at incident energy $E_d = 200 \text{ MeV}$ ($= 3.2 \times 10^{-11} \text{ J}$). Using these values, the acceleration disturbance becomes $f_c = 1.5 \times 10^{-18} \text{ m s}^{-2} \text{ Hz}^{-1/2}$.

5.4. Residual-gas impacts

From the kinetic theory, the number of residual-gas molecules (assumed as ideal gas) that pass an area (A_p) of the proof mass per second is given by $\varpi = n A_p \bar{v} / 6$, where $n = P / (k_B T_P)$ is the number density of the molecules and $\bar{v} = \sqrt{3 k_B T_P m_N^{-1}}$ is the average thermal velocity (P is the pressure of residual gas, $k_B = 1.38 \times 10^{-23} \text{ J K}^{-1}$ is the Boltzmann constant, T_P is the temperature of the proof-mass housing and $m_N = 4.65 \times 10^{-26} \text{ kg}$ is the mass of nitrogen molecules). Assuming the Poisson distribution of the impact rate, we define the spectral density of fluctuations in ϖ as $\delta\varpi(\omega) \equiv \sqrt{2\varpi}$.

Acceleration due to the residual gas impacts is given by $2m_N \varpi \bar{v} m_p^{-1}$ and acceleration disturbance due to fluctuations in the impact rate of residual gas is given by f_{rg} listed in table 3. For $P = 10^{-5} \text{ Pa}$, $A_p = 1.75 \times 10^{-3} \text{ m}^2$ and $T_P = 293 \text{ K}$, we obtain $f_{rg} = 7.4 \times 10^{-16} \text{ m s}^{-2} \text{ Hz}^{-1/2}$. Stebbins et al. use $3 \times 10^{-6} \text{ Pa}$ as the residual gas pressure around the proof mass in the error estimates for LISA [23].

5.5. Radiometric effect

Acceleration disturbance due to the radiometric effect (e.g. [28, 29, 30, 31, 32]) is given by f_{re} listed in table 3, where δT_d is fluctuation in temperature difference across the proof mass housing. This value has to be estimated by carrying out thermal modeling. According to thermal analysis for LISA, temperature fluctuation on the optical bench, to which the proof mass housing is mounted, due to power dissipation of amplifiers is about $3.0 \times 10^{-5} \text{ K Hz}^{-1/2}$ at 1 mHz (table 6.2-28 of [8]). By assuming that the fluctuation rises as $1/\nu$, the temperature fluctuation of the optical bench is $\delta T_{ob} = 3.0 \times 10^{-4} \text{ K Hz}^{-1/2}$ at 0.1 mHz. At the frequency of 0.1 mHz and higher frequencies, the temperature fluctuation on the optical bench would be dominated by the fluctuation in the power dissipation [33]; fluctuation due to solar irradiance at 0.1 mHz is $1.1 \times 10^{-6} \text{ K Hz}^{-1/2}$ (table 6.2-16 of [8]). The ratio $\delta T_{ob} / \delta T_d$ would range from 30 to 100 [33]. By using a value of 30 for the ratio, we obtain $\delta T_d = 1.0 \times 10^{-5} \text{ K Hz}^{-1/2}$ at 0.1 mHz. By using this value, we obtain $f_{re} = 1.7 \times 10^{-16} \text{ m s}^{-2} \text{ Hz}^{-1/2}$ at 0.1 mHz.

5.6. Temperature dependent outgassing effect

Outgassing from walls of the sensor cage is thought to produce greater acceleration noise than the radiometric effect [34, 35]. An analysis done for the LISA Technology Package (LTP), assuming a simple model of flow circuit with a linear approximation, shows that the outgassing effect is nearly 10 times the radiometric effect [35]. By

using this estimate and the estimate we made for the radiometric effect in the previous section, we obtain $f_{og} = 1.7 \times 10^{-15} \text{ m s}^{-2} \text{ Hz}^{-1/2}$ at 0.1 mHz for ASTROD I.

5.7. Thermal radiation pressure

By assuming a perfectly reflecting surface of the proof mass, thermal radiation pressure produces acceleration disturbance (f_{tr} in table 3) due to fluctuations in the temperature difference across the proof-mass housing. In the expression of f_{tr} listed in table 3, $\sigma = 5.7 \times 10^{-8} \text{ W m}^{-2} \text{ K}^{-4}$ is the Stefan-Boltzmann constant, A_p is the area of the proof mass and T_p is the temperature of the proof-mass housing. A factor of one-third is multiplied, as done in the estimation for LISA by Schumaker [13, 14], as a margin for the fact that not all of the radiation momentum is normally incident on the proof mass. For the housing temperature of 293 K and the temperature fluctuation of $1.0 \times 10^{-5} \text{ K Hz}^{-1/2}$, we obtain $f_{tr} = 1.3 \times 10^{-16} \text{ m s}^{-2} \text{ Hz}^{-1/2}$ at 0.1 mHz. The same value was used for the temperature fluctuation in the error estimates for LISA [23].

5.8. Gravity gradients due to thermal distortion of the spacecraft

The temperature fluctuation in solar irradiance would cause fluctuation in distortions of the spacecraft: $\delta x x^{-1} = CTE \cdot |\delta T_{sc}|$, where CTE and δT_{sc} are the coefficient of thermal expansion and temperature fluctuation of the spacecraft, respectively. The inherent fluctuation in solar radiation is $\delta W_0/W_0 = 4\delta T/T_p \approx 2.8 \times 10^{-3} \text{ Hz}^{-1/2}$ at 0.1 mHz [15]. Therefore, the temperature fluctuation is $0.2 \text{ K Hz}^{-1/2}$ for $T_p = 293 \text{ K}$. The gravitational disturbance by a 1-kg mass (M_{dis}) separated from the proof mass in the sensitive axis by $x = 0.5 \text{ m}$ of aluminium structure would be $f_{gg} = 2.7 \times 10^{-15} \text{ m s}^{-2} \text{ Hz}^{-1/2}$ for $\delta T_{sc} = 0.2 \text{ K Hz}^{-1/2}$ and CTE (of Aluminium) = $2.5 \times 10^{-5} \text{ K}^{-1}$. The same disturbing mass ($M_{dis} = 1 \text{ kg}$ and $x = 0.5 \text{ m}$) is assumed in [13, 14, 23]. In reality, the mass to be involved in thermal distortion would be much larger, but the influence would be largely canceled because of the axial symmetry in the original spacecraft geometry. The inherent fluctuation in solar radiation could be reduced largely by thermal shielding. In the estimation for LISA, $\delta T_{sc} = 0.004 \text{ K Hz}^{-1/2}$ is used [14, 23]. For a more accurate estimate, gravity effects by thermal and non-thermal distortions of the spacecraft and the payload have to be studied by appropriate modeling.

6. Proof-mass sensor back-action acceleration disturbances

The total mechanical energy of the capacitive sensing system can be expressed as (e.g. equation (A.3) of [13]):

$$W = -\frac{1}{2} \sum_i C_i (V_i - V_s)^2 + \frac{1}{2} \frac{q^2}{C} + qV_s \quad (10)$$

where q is a net charge of the proof mass; C is the sum of the capacitances due to the applied voltages on the surrounding electrodes i and the potential to ground g : $C = \sum_i C_i$, where $i = x_1, x_2, y_1, y_2, z_1, z_2, g$; V_s is the voltage induced on the proof mass by the applied voltages on the electrodes: $V_s \equiv C^{-1} \sum_i V_i C_i$. The first term of W is the total energy done on the proof mass by the applied voltages of the surrounding electrodes. The second term is the energy acquired on the proof mass by

the image charge on the surrounding electrodes. The third term is the energy stored on the proof mass by the deposit of the free charge on the proof mass.

The x -component of the force on the proof mass is given by differentiation of equation (10) with respect to x . For a simplicity, we assume that neither the free charge q nor the potentials V_i have appreciable gradients along the x -axis, as per [13]. Acceleration disturbances due to fluctuations in the applied voltages and charge can be given by $f_{b1} - f_{b4}$ as listed in table 3. A detailed description on the deviations of $f_{b1} - f_{b4}$ is given in Appendix A of [13]. The parameter values used in this section and the estimated values are listed in tables 1 and 3, respectively.

To simplify the analysis, several assumptions were made in the process of deriving the expressions for the four classes of acceleration disturbances ($f_{b1} - f_{b4}$) [13]: (1) C_i are all comparable with each other in magnitude and on the order of $C_x \approx 6$ pF ($= \epsilon_0 A d^{-1}$, where $\epsilon_0 = 8.9 \times 10^{-12}$ F m $^{-1}$ is the permittivity of vacuum, A is the area of each electrode and $d = 2$ mm is the gap); (2) only the capacitances C_{x1} and C_{x2} have nonzero gradients along the x -axis: $C'_{x1} = -C'_{x2}$, and the gradient of the total capacitance $C \approx 6 C_x$ is: $C' \approx (C_x \Delta d) d^{-2}$, where Δd is the gap asymmetry in the x -direction; (3) the average of the potentials on opposing faces is same for all three axes and expressed as V_{x0} ($\equiv (V_{x1} + V_{x2})/2 = 0.1$ V); (4) the magnitude of the fluctuation in potential δV_i is all identical and take the value of the average fluctuation of all the potentials for the three axes and the voltage to ground. We express the fluctuation as δV_{x0} . It should be noted that we do not consider any cross-talk effects that arise in the sensitive axis due to forces applied to the other degrees of freedom.

6.1. Fluctuations in voltage imbalance and charge

f_{b1} is associated only with sensing voltages but not the free charge, and its value is $f_{b1} \approx 1.4 \times 10^{-15}$ m s $^{-2}$ Hz $^{-1/2}$, by assuming $V_{0g} \equiv V_{x0} - V_g = 0.05$ V. This value is larger than the value used for LISA [23] by a factor of five. Also, we use $\delta V_d = 1.0 \times 10^{-4}$ V Hz $^{-1/2}$ as fluctuation in voltage imbalance V_d ($\equiv V_{x1} - V_{x2} = 0.01$ V). This value (δV_d) is one order of magnitude larger than the value used for LISA [13, 14, 23]. Further, we assume that $C_g/C \approx 1/6$, as per [13, 14].

f_{b2} and f_{b3} arise from fluctuations in the force due to the interaction between the net free charge and applied sensing voltages. f_{b2} is due to fluctuation in voltage imbalance and its value is $f_{b2} \approx -4.8 \times 10^{-15}$ m s $^{-2}$ Hz $^{-1/2}$, where the net free charge on the proof mass is set to the nominal maximum built-up charge, described earlier. f_{b3} is due to fluctuation in charge and its value is $f_{b3} \approx -2.9 \times 10^{-15}$ m s $^{-2}$ Hz $^{-1/2}$. The value of V_d used here is larger than the one used in the error estimates for LISA [23] by a factor of two. f_{b4} is associated only with the free charge and its value is $f_{b4} \approx 4.0 \times 10^{-17}$ m s $^{-2}$ Hz $^{-1/2}$. In the estimation, we assume that the gap asymmetry in the x -direction is $\Delta d = 10$ μ m, which is larger than [13, 14] by one order of magnitude.

6.2. Readout electronics

Readout electronics for the capacitive sensing will be similar to ones studied for LISA (e.g. [36, 37, 38]). For the standard resonant inductive-bridge scheme discussed in [37], the sources of disturbances due to readout electronics can be classified into two categories: imperfections in the capacitance bridge and the electric noise in the detecting circuit. The former includes fluctuations of inductance imbalance ($\Delta L/L$), fluctuations of mutual inductance imbalance ($\Delta M/M$), bias oscillator

relative amplitude noise ($\Delta V/V_{M0}$, where V_{M0} is the 100 kHz bias voltage capacitively applied to the proof mass by injection electrodes on insensitive faces (the y and/or z faces) of the proof mass; the sensing electrodes are grounded) and bias oscillator phase noise ($\Delta\phi$). The latter includes current noise and thermal noise.

Using the expressions for these sources of the disturbances given in table 1 of [37], the main contributions to the acceleration disturbance at 0.1 mHz for ASTROD I are from $\Delta V/V_{M0}$ ($\approx 1.5 \times 10^{-15} \text{ m s}^{-2} \text{ Hz}^{-1/2}$) and $\Delta\phi$ ($\approx 9.1 \times 10^{-16} \text{ m s}^{-2} \text{ Hz}^{-1/2}$), and the thermal noise ($\approx 3.8 \times 10^{-17} \text{ m s}^{-2} \text{ Hz}^{-1/2}$) and the current noise ($\approx 1.3 \times 10^{-17} \text{ m s}^{-2} \text{ Hz}^{-1/2}$). Contributions from fluctuations of $\Delta L/L$ and $\Delta M/M$ are insignificant. In the estimation, we use the following parameters based on experimental results reported in [37]: $\Delta L/L \approx 10^{-4}$, $\Delta M/M \approx 6 \times 10^{-8}$, $\Delta V/V_{M0} \approx 10^{-3} \text{ Hz}^{-1/2}$, $\Delta\phi \approx 5.7 \times 10^{-4} \text{ Hz}^{-1/2}$ and the turn ratio of the transformer $n = 1$ (40 turns, inductance of 5 mH and a quality factor of 165), and a somewhat relaxed residual imbalance of the bridge $\rho_{dc} \approx \Delta d/d = 5 \times 10^{-3}$. This relaxation has resulted in the dominant contributions from the bias oscillator relative amplitude noise and the phase noise. In [37], the thermal noise is dominant as they use $\rho_{dc} \approx 10^{-4}$ in their estimation. The rss of these disturbances is $f_{ba} \approx 1.8 \times 10^{-15} \text{ m s}^{-2} \text{ Hz}^{-1/2}$ at 0.1 mHz and listed in table 3.

6.3. Patch field voltage

Even when the sensing voltages are not applied on the electrodes, differences in local surface properties of the electrodes and the proof mass could lead a potential difference, patch-field voltage, between them [39]. The charge fluctuations δq result in acceleration disturbance f_{pe} (table 3) through the patch field [38]. By taking the average patch-field voltage difference between opposing electrodes as $V_{pe}=0.1 \text{ V}$ [13, 14, 38], we obtain $f_{pe} = 2.9 \times 10^{-14} \text{ m s}^{-2} \text{ Hz}^{-1/2}$ at 0.1 mHz. This is the dominant contribution to the total acceleration disturbance of the ASTROD I proof mass. The LISA study team is investigating the possibility of measuring and compensating voltage differences across capacitors, during the mission commission process, to considerably better than 0.01 V [23].

6.4. Dielectric losses

Dielectric losses are thought to stem from surface contamination of electrodes and produces thermal voltage noise [40, 38]:

$$\delta v_{diel} = \sqrt{4k_B T_p \frac{\delta}{\omega C_x}} \quad (11)$$

where δ is loss angle. The upper limit of δ is reported to be 10^{-5} for Al electrodes [41]. For $\delta = 10^{-5}$, this voltage noise is about $6.6 \mu\text{V Hz}^{-1/2}$ at 0.1 mHz and produces acceleration disturbance f_{dl} (see table 3 for the expression), through residual dc bias voltage on electrodes, in the sensitive axis [40, 38]. By making the same assumption of the average potential difference $V_0 = 0.1 \text{ V}$ between a given electrode and the proof mass as [38], we obtain $f_{dl} \approx 1.6 \times 10^{-15} \text{ m s}^{-2} \text{ Hz}^{-1/2}$. In the error estimates for LISA [23], $V_0 = 0.01 \text{ V}$ is used.

6.5. Summary of the direct acceleration disturbances of the proof mass

By adding in quadrature, the rss of the proof-mass environmental acceleration disturbances (f_{nep}) and the sensor back-action acceleration disturbances (f_{nbp}) are $5.2 \times 10^{-15} \text{ m s}^{-2} \text{ Hz}^{-1/2}$ and $3.0 \times 10^{-14} \text{ m s}^{-2} \text{ Hz}^{-1/2}$, respectively. Therefore, the total direct proof-mass acceleration disturbance (f_{np}) is $3.0 \times 10^{-14} \text{ m s}^{-2} \text{ Hz}^{-1/2}$ at 0.1 mHz, dominated by the sensor back-action acceleration disturbances.

7. Proof mass-spacecraft coupling

The stiffness K is considered to stem from gravity gradients (K_{gg}), fluctuations in sensing capacitance and capacitance gradients (K_{s1} , K_{s2} and K_{s3}), bias voltage (K_{s4}), patch field voltage (K_{s5}) and magnetic field gradients (K_{m1} and K_{m2}). Table 4 gives a summary of estimated values for these sources of stiffness. The expressions used in the estimations are briefly described below. A detailed description on deviations of the expressions for K_{gg} , K_{s1} , K_{s2} , K_{s3} and K_{s5} is given in Appendix A of [13]††.

7.1. Gravity gradients

For a given disturbing point mass (M_{dis}) at a distance x from the center of mass of the proof-mass on the sensitive axis, the amplitude of the acceleration disturbance of the proof-mass caused by a positional fluctuation X_{ps} is $a_{gg} \equiv K_{gg}X_{ps}$, where K_{gg} is given in table 4.

Making the same assumption of $M_{dis} = 0.03 \text{ kg}$ and $x = 0.05 \text{ m}$ as [23], we obtain $K_{gg} \approx 3.2 \times 10^{-8} \text{ s}^{-2}$. For a more detailed analysis, the identification of the disturbing mass is necessary. Gravitational modeling for ASTROD I is in progress [42].

This disturbance arises from any positional fluctuation and is different from the gravity gradient caused by thermal distortion or motion (f_{gg}), which was discussed earlier.

7.2. Fluctuations in capacitive sensing

The expressions for K_{s1} , K_{s2} and K_{s3} can be obtained in the similar way as f_{b1} , f_{b2} , f_{b3} and f_{b4} in the previous section, under the following assumptions [13]: fluctuations in the capacitances C_{x1} and C_{x2} and their derivatives produce disturbing forces in the x -direction, but not the fluctuations in other capacitances or their derivatives; we ignore the cross-coupling effects. Also, we assume $\delta C_{x1} = -\delta C_{x2} \approx (C_x/d)\delta x$ and $\delta C'_{x1} = \delta C'_{x2} \approx (C_x/d^2)\delta x$.

K_{s1} is due to the fluctuations in the Coulomb interaction between the charged proof mass and the image charges on the surrounding electrodes. K_{s2} arises from interaction between the net free charge q on the proof-mass and the average electrode voltages. K_{s3} is due to the applied voltages across electrodes and the voltage difference across opposite electrodes. The estimated values for K_{s1} , K_{s2} and K_{s3} are given in table 4.

7.3. Bias voltage

By assuming that the sensing electrodes are grounded, the dominant term of the readout stiffness along the sensitive axis is given by K_{s4} [38], listed in table 4.

†† K_{s5} in text is noted as K_{s4} in [13].

Table 4. The proof-mass stiffness in units of 10^{-9} s^{-2} (see sections 6 and 7, and tables 1 and 2 for notation.)

[10^{-9} s^{-2}]		Expressions	ASTROD I
K_{gg}	Gravity gradients	$2 \frac{GM_{dis}}{x^3}$	32
K_{s1}	Image charges	$\frac{1}{m_p C d^2} \left(\frac{C_x}{C} \right) q^2$	0.66
K_{s2}	$q \times V_{0g}$	$\left(\frac{2}{m_p d^2} \right) \left(\frac{C_x}{C} \right) \left(\frac{C_q}{C} \right) q V_{0g}$	0.40
K_{s3}	Applied voltages	$\frac{C_x}{m_p d^2} \left\{ \left(\frac{C_x}{C} + \frac{1}{4} \right) V_d^2 + \left(\frac{C_q}{C} \right)^2 V_{0g}^2 \right\}$	0.095
K_{s4}	Bias voltage	$\frac{C_x}{m_p d^2} V_{M0}^2$	3.1×10^2
K_{s5}	Patch fields	$\gamma \left(\frac{C_x}{m_p d^2} \right) \left(\frac{C_q}{C} \right)^2 V_{pe}^2$	1.2
K_{m1}	Induced magnetic moments	$\frac{2\chi m}{\rho\mu_0} \{ \vec{\nabla} B_{sc} ^2 + B_{sc} \vec{\nabla}^2 B_{sc} \}$	9.0×10^{-5}
K_{m2}	Magnetic remanent moments	$\frac{1}{\sqrt{2} m_p} \vec{M}_r \vec{\nabla}^2 B_{sc} $	6.9×10^{-4}
rss($K_{gg} - K_{m2}$) $\equiv K$			3.1×10^2

Assuming, as per [38], that the proof mass is biased to $V_{M0} = 0.6 \text{ V}$, $K_{s4} \approx 3.1 \times 10^{-7} \text{ s}^{-2}$.

7.4. Patch field voltage

By assuming a nominal patch-field voltage of $V_{pe} = 0.1 \text{ V}$ [13, 14, 38] and an overall multiplicative factor of $\gamma = 5$ as per [13, 14], the contribution due to the patch field to the proof mass-spacecraft coupling is $K_{s5} \approx 1.2 \times 10^{-9} \text{ s}^{-2}$ (table 4).

7.5. Magnetic field gradients

The magnetic stiffness is given by $K_m = \frac{1}{m_p} \vec{\nabla} [\vec{\nabla} (\vec{M}_p \cdot \vec{B})]$ [18]. The expressions for dominant terms of the stiffness due to the induced magnetic moment and the remanent moment are given by K_{m1} and K_{m2} (as listed in table 4), respectively, where $|\vec{\nabla}^2 B_{sc}| \approx 12 B_{sc} r_m^{-2} = 1.7 \times 10^{-5} \text{ T m}^{-2}$ for $r_m = 0.75 \text{ m}$. Their contributions to the total stiffness are insignificant.

7.6. Summary of the estimated values of stiffness

These contributions to the coupling constant K are summarized in table 4. The rss of the coupling constant is $3.1 \times 10^{-7} \text{ s}^{-2}$. This is slightly below the requirement for the total stiffness in LISA ($4 \times 10^{-7} \text{ s}^{-2}$ [38]).

8. Requirements for the readout sensitivity and spacecraft control-loop gain

We have estimated values for the coupling constant K , the direct spacecraft acceleration disturbance f_{ns} and the direct proof-mass acceleration disturbance f_{np} . By using the expression for the total acceleration disturbance of f_p (equation (8)), we infer the requirements for the readout sensitivity X_{nr} and the spacecraft control-loop gain u . In this process, we allocate an identical magnitude f_a to each term

of the expression; $f_a^2 = f_p^2/3$. For ASTROD I, the noise goal is $10^{-13} \text{ m s}^{-2} \text{ Hz}^{-1/2}$ at 0.1 mHz and, therefore, $f_a = 5.8 \times 10^{-14} \text{ m s}^{-2} \text{ Hz}^{-1/2}$. The second term of the expression is f_{np} , which was estimated to be $3.0 \times 10^{-14} \text{ m s}^{-2} \text{ Hz}^{-1/2}$ (table 3); it is about a factor of 2 smaller than the allocated requirement. With the estimated total stiffness $K = 3.1 \times 10^{-7} \text{ s}^{-2}$, we obtain $X_{nr} \leq 1.9 \times 10^{-7} \text{ m Hz}^{-1/2}$ from the first term and $u \geq 3.8 \times 10^5$ from the last term of the expression.

From figure 1, one can see that the acceleration noise spectral density requirements for ASTROD I take its lowest value of about $0.4 \times 10^{-13} \text{ m s}^{-2} \text{ Hz}^{-1/2}$ at 0.3 mHz. At this frequency, f_a becomes $2.3 \times 10^{-14} \text{ m s}^{-2} \text{ Hz}^{-1/2}$. Therefore, the requirement for X_{nr} becomes more stringent at 0.3 mHz: $X_{nr} \leq 7.4 \times 10^{-8} \text{ m Hz}^{-1/2}$. As for the second term of f_p , f_{np} is smaller at higher frequencies [13, 14]. Our estimate of f_{np} is dominated by the contribution from f_{pe} , which scales as ν^{-1} . Therefore, at 0.3 mHz, f_{np} would be $\sim 1 \times 10^{-14} \text{ m s}^{-2} \text{ Hz}$, which is smaller than f_a at 0.3 mHz. The last term scales as ω^{-2} , and f_{ns} is expected to be smaller at higher frequencies because of the $\nu^{-1/3}$ dependence of the fractional fluctuation in solar irradiance (figure 6 of [15]). Therefore, by assuming the same level of the thruster noise, the requirement for u at 0.3 mHz would be less stringent than that at 0.1 mHz by a factor of ~ 4 .

In summary, the requirements for the readout sensitivity and the control loop gain for ASTROD I are $X_{nr} \leq 7.4 \times 10^{-8} \text{ m Hz}^{-1/2}$ and $u \geq 3.8 \times 10^5$, respectively.

9. Comparison with LISA

Main relaxed parameter-values are listed in table 5 in comparison with LISA. The values for LISA are quoted from the current error estimates by Stebbins et al. [23], except the thruster noise quoted from [7]. Recently the LISA requirements for the thruster noise and the residual gas pressure have been relaxed further from the values given in table 5 (this is a comment from one of the referees).

Table 5. Relaxed parameter values in comparison with LISA

$\nu = 0.1 \text{ mHz}$	ASTROD I	LISA
Maximum charge build-up: q [C]	10^{-12}	10^{-13}
Magnetic susceptibility: χ_m	5×10^{-5}	3×10^{-6}
Magnetic remanent moment: $ \vec{M}_r $ [A m ²]	1×10^{-7}	2×10^{-8}
Residual gas pressure: P [Pa]	10^{-5}	3×10^{-6} ^b
Electrostatic shielding factors: ξ_e	10	100
Thruster noise [$\mu\text{N Hz}^{-1/2}$]	10	a few
Fluctuation of temperature in SC: δT_{sc} [K Hz ^{-1/2}]	0.2	0.004
Voltage difference between average voltage across opposite faces and voltage to ground: V_{0g} [V]	0.05	0.01
Voltage difference between opposing faces: V_d [V]	0.01	0.005
Fluctuation of voltage difference across opposite faces: δV_d [V Hz ^{-1/2}]	10^{-4}	10^{-5}
Residual dc bias voltage on electrodes: V_0 [V]	0.1	0.01

^b According to one of the referees, this LISA requirement has been relaxed to 10^{-5} Pa .

Table 6. Acceleration disturbances and requirements. PM and SC denote proof-mass and spacecraft, respectively.

ASTROD I	
(a) Estimated total acceleration disturbance (at 0.1 mHz): f_p [m s ⁻² Hz ^{-1/2}]	8.7×10^{-14}
(b) Estimated contributions to f_p (at 0.1 mHz): $f_p \approx X_{nr}(-K) + f_{np} + (f_{ns} + TN_t)K\omega^{-2}u^{-1}$	
Direct PM acceleration disturbances: f_{np} [m s ⁻² Hz ^{-1/2}]	3.0×10^{-14}
Direct SC acceleration disturbances: $f_{ns} + TN_t$ [m s ⁻² Hz ^{-1/2}]	2.8×10^{-8}
PM-SC spring constant: K [s ⁻²]	3.1×10^{-7}
(c) Inferred requirements	
Position readout noise: X_{nr} [m Hz ^{-1/2}]	7.4×10^{-8}
Control-loop gain: u	3.8×10^5

10. Summary, discussion and conclusions

We have estimated the spacecraft acceleration disturbance f_{ns} (section 4), the proof-mass acceleration disturbances f_{np} (sections 5 and 6) and the stiffness K between the spacecraft and the proof mass (section 7). By using the expression (8), we have inferred the requirements for the readout sensitivity X_{nr} and the control-loop gain u (section 8).

Table 6 provides a summary of the estimated acceleration disturbances and the stiffness (section (b)), and the requirements (section (c)). The estimated total acceleration disturbance f_p at 0.1 mHz (section (a) of table 6) is about 13 % less than the noise goal of 10^{-13} m s⁻² Hz^{-1/2}. We have compared the parameter values used in the estimation with LISA in section 9.

The total direct acceleration disturbance of the proof mass (f_{np}) at 0.1 mHz was estimated to be nearly a factor of two smaller than the requirement. This ~ 50 % margin may be allocated for unknown disturbances or disturbances that would arise but have not been studied yet. These unestimated disturbances would be originated from, for instance, cross-talks in the capacitive sensing and magnetic damping of the proof mass. An estimate of acceleration disturbance due to magnetic damping for LISA is about 2×10^{-16} m s⁻² Hz^{-1/2} at 0.1 mHz [23]. The contribution from the magnetic damping effect to ASTROD I would be in the similar order and insignificant.

The sensor back-action acceleration disturbances can be reduced by increasing the magnitude of the gap d . The total stiffness K would be also reduced, for example, by a factor of four by changing the gap to 4 mm. The optimum design for the capacitive sensing is to be discussed based on results from the ongoing laboratory torsion balance experiment for ASTROD I [43].

Parameter values we used in this paper are mainly based on the results of studies done for LISA and LISA Pathfinder. This may be sufficient for the preliminary estimation. More accurate estimation would be obtained by carrying out the following works dedicated for ASTROD I: (a) modeling local magnetic fields of the spacecraft, (b) estimating the effective charging rate of the proof-mass, (c) estimating the cosmic-ray impact rate of the proof-mass, (d) estimating the micrometeorite impact effects,

(e) thermal modeling of the proof-mass housing and the spacecraft, (f) gravitational modeling that includes thermal and non-thermal deformation of the spacecraft and the payload, (g) electrostatic modeling for the capacitive sensors and (h) estimating environmental factors (such as the interplanetary magnetic field, solar wind, solar radiation and cosmic rays) in the varying orbit (0.5 AU to 1 AU). Simulations to estimate charging rates for ASTROD I are in progress [27].

We have tentatively estimated acceleration disturbances for ASTROD I. This work has allowed us to set preliminary requirements for ASTROD I. To improve the current estimation, the disturbances that have not been studied yet have to be included and more detailed modeling works are necessary for ASTROD I. In comparison with LISA, requirements for ASTROD I can be largely relaxed. This will make the technological developments for ASTROD I less demanding to meet the drag-free requirements.

Acknowledgments

This work was funded by the National Science Council and the Foundation of Minor Planets of Purple Mountain Observatory. We thank A. Rüdiger, S. Vitale, D. K. Gill, A. Pulido Patón, and, especially, the referees for useful information on acceleration disturbances and helpful comments on the manuscript.

References

- [1] Bec-Borsenberger A *et al* 2000 *ASTROD* ESA F2/F3 Mission Proposal; and references therein
- [2] Ni W-T 2002 *Int. J. Mod. Phys. D* **11** 947; and references therein
- [3] Ni W-T *et al* 2002 *Int. J. Mod. Phys. D* **11** 1035; and references therein
- [4] Ni W-T *et al* 2003 ASTROD I: Mission Concept and Venus Flybys, *Proc. 5th IAA Intl. Conf. On Low-Cost Planetary Missions, ESTEC, Noordwijk, The Netherlands, 24-26 September 2003*, ESA SP-542, pp. 79-86, November 2003; *Acta Astronaut.* in press, 2006
- [5] Xia Y, Ni W-T, Tang C J and Li G 2006 Orbit Design and Orbit Simulation for ASTROD I, *Gen. Relat. Gravit.* **38**, in press
- [6] Anza S *et al* 2005 *Class. Quantum Grav.* **22** S125
- [7] *LISA system and technology study report* 2000 ESA-SCI(2000)11
- [8] Hammesfahr A *et al* 2000 *LISA-Study of the Laser Interferometer Space Antenna, Final Technical Report* ESA Industrial Study at Phase A, ESTEC contract no. 13631/99/NL/MS, DSS Report no. LI-RP-DS-009
- [9] Vitale S *et al* 2005 *Science Requirements and Top-level Architecture Definition for the Lisa Technology Package (LTP) on Board LISA Pathfinder (SMART-2)* LTPA-UTN-SsRD-Iss003-Rev1 June 30, 2005
- [10] Ni W-T, Shiomi S and Liao A-C 2004 *Class. Quantum Grav.* **21** 641
- [11] Vitale S and Dolesi R 2000 CP523 *Gravitational Waves: Third Edoardo Amaldi Conference*, ed Meshkov S, American Institute of Physics 1 56396-944-0 231
- [12] Vitale S *et al* 2002 *Nucl. Phys. B (Proc. Suppl.)* **110** 209
- [13] Schumaker B L 2002 Overview of Disturbance Reduction Requirements for LISA <http://elmer.tapir.caltech.edu/ph237/week18/DRS-bls01May02.pdf>
- [14] Schumaker B L 2003 *Class. Quantum Grav.* **20** S239
- [15] Pap J *et al* 1999 *Adv. Space Res.* **24**, No.2 215
- [16] Fichter W, Gath P, Vitale S and Bortoluzzi D 2005 *Class. Quantum Grav.* **22** S139
- [17] Jackson J D 1998 *Classical electrodynamics*, 3rd ed., John Wiley & Sons, Inc.
- [18] Hanson J *et al* 2003 *Class. Quantum Grav.* **20** S109
- [19] Lang K R 2001 *The Cambridge Encyclopedia of the Sun*, Cambridge University Press
- [20] Balogh A *et al* 1992 *Astron. Astrophys. Suppl. Ser.* **92** 221
- [21] Shaul D N A *et al* 2005 *Class. Quantum Grav.* **22** S297
- [22] Silvestri Z *et al* 2003 *Metrologia* **40** 172-176
- [23] Stebbins R T *et al* 2004 *Class. Quantum Grav.* **21** S653

- [24] Gill D K, Private communication, January 2006
- [25] Jafry Y and Sumner T J 1997 *Class. Quantum Grav.* **14** 1567
- [26] Araújo H M *et al* 2004 Detailed Calculation of Test-Mass Charging in the LISA Mission [airXiv:astro-ph/0405522](https://arxiv.org/abs/astro-ph/0405522) v3 7 Oct 2004, published in *Astroparticle Physics* **22** 2005 451
- [27] Bao G *et al* 2006 ASTROD I Charging Simulation and Disturbances *Gen. Relat. Gravit.* **38**, in press
- [28] Blaser J P, Lockerbie N, Paik H J, Speake C and Vitale S 1996 *Class. Quantum Grav.* **13** A203
- [29] Touboul P, Rodrigues M, Willemenot E and Bernard A 1996 *Class. Quantum Grav.* **13** A67
- [30] Nobili A M *et al* 2001 *Phys. Rev. D* **63** 101101(R)
- [31] Worden P, Mester J and Torii R 2001 *Class. Quantum Grav.* **18** 2543
- [32] Rodrigues M, Foulon B, Liorzou F and Touboul P 2003 *Class. Quantum Grav.* **20** S291
- [33] Bender P 2003 *Class. Quantum Grav.* **20** S301
- [34] Rüdiger A 2002 Residual gas effects in space-borne position sensors http://eotvos.dm.unipi.it/nobili/opendiscussion/ruediger_30aprile.pdf
- [35] Dolesi R *et al* 2003 *Class. Quantum Grav.* **20** S99
- [36] Speake C C and Andrews P L 1997 *Class. Quantum Grav.* **14** 1557
- [37] Cavalleri A *et al* 2001 *Class. Quantum Grav.* **18** 4133
- [38] Weber W J *et al* 2003 *Proc. SPIE Conf. on Astronomical Telescopes and Instrumentation* **4856** ed Cruise M and Saulson P (Bellingham WA: SPIE Optical Engineering Press) 31
- [39] Speake C C 1996 *Class. Quantum Grav.* **13** A291-A297
- [40] Vitale S and Speake C C 1998 *2nd LISA Symposium AIP Proceedings* **456**, 172
- [41] Speake C C, Davis R S, Quinn T J and Richman S J 1999 *Phys. Lett. A* **263** 219
- [42] Shiomi S 2005 Acceleration disturbances due to local gravity gradients in ASTROD I, *Proceedings of the 6th Edoardo Amaldi Conference on Gravitational waves* (Okinawa, Japan, June 20-24, 2005); 2006 *J. Phys.:Conf. Ser.* **32** 186
- [43] Zhou Z B, Gao S W and Luo J 2005 *Class. Quantum Grav.* **22** S537